PAPER

Range and Size Estimation Based on a Coordinate Transformation Model for Driving Assistance Systems

Bing-Fei WU[†a)], ***Member***, **Chuan-Tsai LIN**[†], ***Nonmember***, ***and*** **Yen-Lin CHEN**[††], ***Member***

SUMMARY This paper presents new approaches for the estimation of range between the preceding vehicle and the experimental vehicle, estimation of vehicle size and its projective size, and dynamic camera calibration. First, our proposed approaches adopt a camera model to transform coordinates from the ground plane onto the image plane to estimate the relative position between the detected vehicle and the camera. Then, to estimate the actual and projective size of the preceding vehicle, we propose a new estimation method. This method can estimate the range from a preceding vehicle to the camera based on contact points between its tires and the ground and then estimate the actual size of the vehicle according to the positions of its vertexes in the image. Because the projective size of a vehicle varies with respect to its distance to the camera, we also present a simple and rapid method of estimating a vehicle's projective height, which allows a reduction in computational time for size estimation in real-time systems. Errors caused by the application of different camera parameters are also estimated and analyzed in this study. The estimation results are used to determine suitable parameters during camera installation to suppress estimation errors. Finally, to guarantee robustness of the detection system, a new efficient approach to dynamic calibration is presented to obtain accurate camera parameters, even when they are changed by camera vibration owing to on-road driving. Experimental results demonstrate that our approaches can provide accurate and robust estimation results of range and size of target vehicles.

key words: *camera model, calibration, position estimation, driving assistant, vehicle*

1. Introduction

Accurate and real-time detection of vehicle position, speed and traffic flows are important issues for driving assistance systems and traffic surveillance systems [1]–[4]. During the detection, errors often arise because of camera vibration and constraints such as the limitations of image resolution, quantization errors, and lens distortions [5], [6]. Therefore, accurate error estimation is important in vehicle detection issues, and image processing techniques for position estimation or motion detection are necessary in many situations [7]–[10]. However, most of the previous studies have not involved methods of reducing errors caused by changes of camera parameters, while some important issues like error estimation and the way to set appropriate camera parameters were seldom considered. This may influence the determination of camera parameters and the specifications of a detection system. Therefore, in this paper, we propose an effective strategy to reduce errors of range estimation by determining the most suitable camera parameters.

Previous studies often adopted laser, radar or computer vision techniques in range estimation issues. For example, Chen [11] presented a radar-based detector to find obstacles in the forward collision warning system, where a vision-based module was adopted to confirm that the detected object is not an overhead structure and so avoid false alarms of the warning system. Segawa et al. [12] developed a preceding vehicle detection system for collision avoidance by using a combination of stereo images and non-scanning millimeter-wave radar. In Hautiere et al.'s method [13], a depth map of the road environment is computed and applied for detecting the vertical objects on the road. Stereo-vision based techniques can also be applied on range estimation. By comparing the disparities of two images, obstacles can be detected and their distance to the experimental vehicle can also be estimated [13], [14]. However, the methods above need multiple cameras or at least one set of radar to detect obstacles and estimate the range. If only one single camera is required, the cost and the complexity of the system will be significantly decreased. Nevertheless, the estimation results of a single camera are often influenced by external camera parameters and thus serious errors arise. For example, an outdoor camera is often affected by the wind or rain. Furthermore, camera parameters vary with the pressure of tires, unbalanced load or bumpy roads when the camera is mounted on a moving vehicle. Therefore, automatic calibration is necessary to deal with the above issues. Studies of camera calibration usually adopted points in the world coordinates or certain distinctive patterns [15]–[17]. For instance, Wang and Tsai [15] proposed a camera calibration approach using a planar hexagon pattern drawn on the ground. However, this approach may only be suitable for calibration of fixed cameras. Schoepflin and Dailey [16] supposed the camera swing angle was zero and searched for the vanishing point by extending lane markings in the image to calibrate the tilt angle. Nevertheless, when the camera swing angle is not zero, errors may arise. Liang, et al. [17] calibrated the tilt angle of a moving camera with the coordinate of the vanishing point. However, the assumption of vehicles staying in the center of lanes may not be reasonable under typical driving conditions and thus such methods may cause more errors on roads with curves. Therefore, it would be better if calibration targets are objects available on the road and errors caused by incomplete assumptions were

Manuscript received June 13, 2008.
Manuscript revised February 24, 2009.

[†]The authors are with Electrical and Control Engineering, National Chiao Tung University, Hsinchu, 30050 Taiwan.
[††]The author is with Computer Science and Information Engineering, National Taipei University of Technology, Taipei 10608,Taiwan.
a) E-mail: bwu@cssp.cn.nctu.edu.tw

DOI: 10.1587/transinf.E92.D.1725

estimated. In fact, camera intrinsic parameters are usually fixed while extrinsic parameters such as angles and heights are variable. Intrinsic parameters can be obtained by analyzing a sequence of images captured by cameras [18]–[21] To solve the problem of changing extrinsic parameters, we propose an approach of automatic calibration to provide robust range estimation for vision-based systems.

Object features, like sizes and shapes, are widely employed in the recognition of objects [22]–[27]. Yilmaz et al. [22] adopted a method of contour-based object tracking to detect pedestrians and to solve the problem of occlusion between objects. Lin et al. [23] computed the number of people in crowded scenes by detecting features of human heads. Pang et al. [24] analyzed vehicle projections with geometry and divided their occlusions in the images to provide essential information to the traffic surveillance systems. Broggi et al. [25] utilized inverse perspective mapping to transfer images of the front driving lanes into a bird's view of parallel lanes to detect and identify vehicles with a bounding box. However, most of the above-mentioned approaches may need the prior information about the projective size and shape of the target object, and it may not be possible to obtain this information accurately and rapidly in many situations. Moreover, the loss of dimensional information during the transformation from 3-D coordinates to 2-D image coordinates often increases difficulties in estimating the projective size and shape of the target object. To solve the problem, we regard a vehicle as a cuboid and with the world coordinates of the cuboid's vertex on the ground, we can estimate the world coordinates of other vertices in the cuboid, determine their projective positions and estimate the size of the cuboid. Since vehicle sizes are within certain ranges, cuboids on the drive lanes whose sizes fit general vehicle sizes should be vehicles. So our method can be applied to vehicle recognition.

In our previous studies [8], [28], [29], we searched for objects with vehicle-like contours and sizes and then estimated their ranges to the experimental vehicle. In this study, we apply error estimation to determine proper camera parameters and then estimate actual and projective sizes of target objects to facilitate vehicle recognition. An approach to rapidly compute projective sizes is also proposed to significantly reduce computation cost of vehicle detection process for real-time and embedded systems. Then, a dynamic calibration approach is presented to calibrate the tilt and swing angles of the camera with information of lane markings and vehicles in the image. The experimental results demonstrate that our work can provide accurate and robust range and size estimation of target vehicles. The content is organized as follows: Section 2 presents rapid size estimation and position estimation of a cuboid on the ground. Section 3 explores range estimation and error estimation with various camera parameters. Section 4 proposes a dynamic calibration approach to deal with the problem of camera vibration and variation in camera angle. Section 5 displays experimental results of range and height estimation, dynamic calibration of camera angles, and comparisons with other approaches. Section 6 provides the conclusion.

2. Position and Size Estimation Using Projective Geometry

The position of any point in the 3-D world coordinates (X, Y, Z) projected to a 2-D image plane (x, y) can be calculated through perspective transformation [15]. Mapping a 3-D scene onto the 2-D image plane is a many-to-one transformation. However, mapping a point on the front horizon of the camera onto an image plane is a one-to-one transformation. Therefore, the relative position between the camera and any point on the ground can be estimated by the coordinate transformation between image plane and ground plane.

2.1 Coordinates Transformation Model

Figure 1 shows the coordinate transformation between image plane and ground plane, where D denotes the origin of the world coordinates (X, Y, Z), and O represents the origin of the image coordinates (u, v). Let λ be the focal length of the camera; L denote the lens center;h represent the height. As shown in Fig. 2 (a), there is a cuboid C associated with a target object, whose lengths, widths and heights are L_1, W_1, and H_1, respectively. Let $P_1(X, 0, Z)$ be located on the ground, then $P_2 = (X, H_1, Z)$, $P_3 = (X + W_1, 0, Z)$, and $P_5 = (X, 0, Z + L_1)$, which is inferred from the size of C. Other vertices can be estimated in the same way. Based on the cuboid's size and the position of its vertex, P_1, the projective positions of other vertices in a cuboid can be estimated to accurately estimate the contour and size of the cuboid's projection.

Figure 2 (b), (c) presents the side view and top view of the image formation. In the figure, tilt angle α denotes the angle between the Z-axis and the optical axis, $\overline{LE}$. $P_1(X, 0, Z)$ projects onto $i_1(u, v)$ on the image plane, and the transformation between the two coordinates can be expressed as (1) and (2) by applying trigonometric function properties and our previous study [6], where $\|Z\|$ and $\|X\|$ respectively denote the range and lateral position between P_1 and the camera.

$$Z(v) = h \cdot \tan\left(\left(\frac{\pi}{2} - \alpha\right) - \tan^{-1}\left(\frac{v}{\lambda}\right)\right) \tag{1}$$

$$X(u, v) = -\frac{u}{\lambda} \times h \cdot \tan\left(\left(\frac{\pi}{2} - \alpha\right) - \tan^{-1}\left(\frac{v}{\lambda}\right)\right) \tag{2}$$

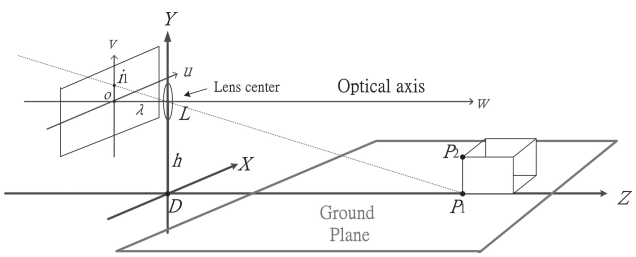

Fig. 1 Coordinate transformation between image plane and ground plane.

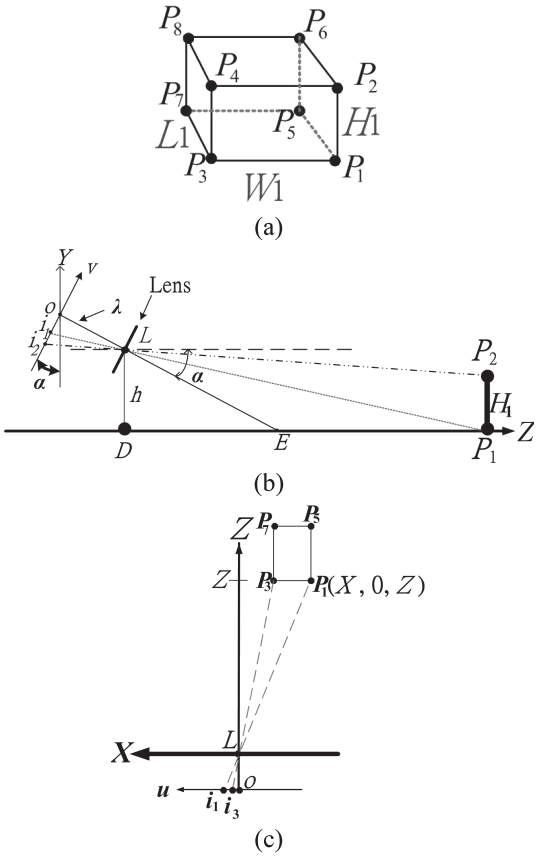

Fig. 2 The projective geometry of a camera model. (a) A cuboid C. (b) Side view. (c) Top view.

Let P_2 and P_3 respectively project onto $i_2(u_2, v_2)$ and $i_3(u_3, v_3)$. The $\overline{P_1P_2}$ is the height of cuboid C, whose projective height is h_{i12} in (3). The distance between P_1 and P_3 is the width of C ; its projective width is w_{i13} in (4).

Based on (1)–(4), if P_1 of the cuboid can be found in the image, then the position and size of the cuboid can be estimated. Likewise, the relation between v_2 and H_1 can be obtained by (3), as shown as (5). Further by applying (5), we can have the height of the cuboid C as in (6).

$$h_{i12} = v - v_2, \tag{3}$$

where $v(Z) = \lambda \times \tan\left[\left(\frac{\pi}{2} - \alpha\right) - \tan^{-1}\left(\frac{Z}{h}\right)\right]$, $v_2(Z) = \lambda \times \tan\left[\left(\frac{\pi}{2} - \alpha\right) - \tan^{-1}\left(\frac{Z}{h - H_1}\right)\right]$

$$w_{i13} = W_1 \times \frac{\lambda}{Z} \tag{4}$$

$$v_2 = \lambda \cdot \left\{ \frac{\tan\left(\frac{\pi}{2} - \alpha\right) - \left(\frac{Z}{h - H_1}\right)}{1 + \tan\left(\frac{\pi}{2} - \alpha\right) \times \left(\frac{Z}{h - H_1}\right)} \right\} \tag{5}$$

$$H_1 = \left(h \cdot \tan\left(\frac{\pi}{2} - \alpha\right) - Z - \frac{v_2 \cdot \left(Z \cdot \tan\left(\frac{\pi}{2} - \alpha\right) - h\right)}{\lambda} \right) \times \left(\frac{\lambda}{\lambda \cdot \tan\left(\frac{\pi}{2} - \alpha\right) - v_2} \right) \tag{6}$$

2.2 Rapid Estimation of Projective Height

A cuboid's projective size varies with its relative position with the camera. From (3), we can estimate its projective height. When applied to driving assistance, the rapid size estimation of the front vehicle's projection can provide helpful information for vehicle recognition and determination of vehicle size.

$$v(Z) = \lambda \left\{ \frac{h \cdot \tan\left(\frac{\pi}{2} - \alpha\right) - Z}{h + Z \cdot \tan\left(\frac{\pi}{2} - \alpha\right)} \right\} \tag{7}$$

From (1), we can obtain the relation between Z and v as shown in (7). In Fig. 2 (b), there is an object whose height is H_1. Therefore, supposing that $P_1(X, 0, Z)$ projects onto $i_1(u, v)$, we can re-write (3) to turn $h_{i12}(v)$ into a linear equation shown in (8). Since the camera is mounted on an experimental vehicle for object detection, when α is too large, the farther part of the lane will not appear in the image. Therefore, α is usually between 0–6 degrees. Also, the height of the camera is restricted by the height of the vehicle roof, to be lower than 1.5 meters. Furthermore, the range Z of the preceding vehicle is usually over 10 m, and thus we can obtain (9) and (10). Then, substitute (9) and (10) into (8) to get (11). Also, by substituting (1) into (11), we obtain $h_{i12}(v)$ as shown in (12). Equation (13) means the first derivative for v to $h_{i12}(v)$. Let $\xi = (\pi/2 - \alpha)$, and $\tau = \tan^{-1}(v/\lambda)$. (15), (16) and (17) derive from (13) and (14). In this study, let $\alpha < 6^\circ$, so $\xi > 84^\circ$, to get (18) and (19). Then they are substituted to (17) to obtain (20) and (21). (21) shows the first derivative of $h_{i12}(v)$ is a constant. Therefore, the relation between the projective height of $\overline{P_1P_2}$, $h_{i12}(v)$, and the projected v-coordinate of P_1 can be expressed by a linear equation as (22).

$$h_{i12}(v) = \lambda \left\{ \frac{h \cdot \tan\left(\frac{\pi}{2} - \alpha\right) - Z}{h + Z \cdot \tan\left(\frac{\pi}{2} - \alpha\right)} - \frac{(h - H_1) \cdot \tan\left(\frac{\pi}{2} - \alpha\right) - Z}{(h - H_1) + Z \cdot \tan\left(\frac{\pi}{2} - \alpha\right)} \right\} \tag{8}$$

$$h + Z \cdot \tan\left(\frac{\pi}{2} - \alpha\right) \cong Z \cdot \tan\left(\frac{\pi}{2} - \alpha\right) \tag{9}$$

$$(h - H_1) + Z \cdot \tan\left(\frac{\pi}{2} - \alpha\right) \cong Z \cdot \tan\left(\frac{\pi}{2} - \alpha\right) \tag{10}$$

$$h_{i12}(v) \cong \frac{H_1 \times \lambda}{Z} \tag{11}$$

$$h_{i12}(v) \cong \frac{H_1 \times \lambda}{h \cdot \tan\left(\left(\frac{\pi}{2} - \alpha\right) - \tan^{-1}\left(\frac{v}{\lambda}\right)\right)} \tag{12}$$

$$\frac{dh_{i12}(v)}{dv} \cong \frac{H_1 \times \lambda}{h} \times \frac{d\cot\left(\left(\frac{\pi}{2} - \alpha\right) - \tan^{-1}\left(\frac{v}{\lambda}\right)\right)}{dv} \tag{13}$$

$$\cot(\xi - \tau) = \frac{1 + \tan(\xi) \times \tan(\tau)}{\tan(\xi) - \tan(\tau)} \tag{14}$$

$$\frac{dh_{i12}(v)}{dv} \cong \frac{H_1 \times \lambda}{h} \times \frac{\left(\tan(\xi) - \frac{v}{\lambda}\right) \times \frac{\tan(\xi)}{\lambda} - \left(1 + \tan(\xi) \times \frac{v}{\lambda}\right) \times \left(-\frac{1}{\lambda}\right)}{\left(\tan(\xi) - \frac{v}{\lambda}\right)^2} \tag{17}$$

$$\tan(\xi) \gg \frac{v}{\lambda} \tag{18}$$

$$\tan(\xi) \times \frac{\tan(\xi)}{\lambda} \gg \left(\frac{v}{\lambda^2} \times \tan(\xi) + \frac{1}{\lambda}\right) \tag{19}$$

$$\frac{dh_{i12}(v)}{dv} \cong \frac{H_1 \times \lambda}{h} \times \frac{(\tan(\xi)) \times \frac{\tan(\xi)}{\lambda}}{(\tan(\xi))^2} \tag{20}$$

$$\frac{dh_{i12}(v)}{dv} \cong \frac{H_1}{h} \tag{21}$$

$$h_{i12}(v) \cong \frac{H_1}{h} \times v + C_1 \tag{22}$$

where C_1 is a constant.

From the sequential images, we get the actual projective height of $\overline{P_1P_2}$. Let the projective height of $\overline{P_1P_2}$ be $h_{i12}(v_a)$ when P_1 projects onto v_a, and the height be $h_{i12}(v_b)$ when projecting onto v_b. Then, by substituting the obtained $h_{i12}(v_a)$ and $h_{i12}(v_b)$ into (22), C_1 and H_1 can be obtained as expressed in (23), (24).

$$H_1 \cong \frac{h \cdot [h_{i12}(v_a) - h_{i12}(v_b)]}{(v_a - v_b)} \tag{23}$$

$$C_1 \cong h_{i12}(v) - \frac{H_1}{h} \times v \tag{24}$$

By comparing (3) and (22), we can find that the proposed approach of projective height estimation significantly reduces the computation cost. Also, the comparison between (6) and (23) shows that the proposed approach requires much less computation timing for estimating the actual height of the target object.

3. Range and Error Estimation

Inaccurate camera parameters often cause estimation errors. Even if the parameters are initially set accurately, they could be changed by external forces, or by the use of mechanical devices, causing the estimated value to be different from the real value. The range estimation results are discussed below.

3.1 Digitalized Equation of Range Estimation

To estimate range with a single camera, the equation evolved by the camera model should be digitalized first. Therefore, an affine transformation from real image coordinates (u, v) to bitmap image coordinates (M, N) can be obtained by (25). Figure 3 displays the relationship between the M-N bitmap image coordinates and the u-v real image coordinates, where the left bottom images denotes the origin $Q(0, 0)$.

$$M = -d_x^{-1} \times u + M_m/2, N = -d_y^{-1} \times v + N_n/2, \tag{25}$$

where d_x and d_y are respectively horizontal and vertical physical distances between adjacent pixels, and the frame size is M_m by N_n pixels.

The relation between N-coordinates and v-coordinates is shown in (25). Substitute (25) into (1), we have the coordinate transformation of Z and N as shown in (26), which is the digitalized equation of range estimation.

$$Z = h \cdot \tan\left(\left(\frac{\pi}{2} - \alpha\right) - \tan^{-1}\left(\frac{((N_n/2) - N) \times d_y}{\lambda}\right)\right) \tag{26}$$

The Range Estimation is analyzed as follows. This study utilized a Hitachi KP-F3 camera with a physical pixel size of

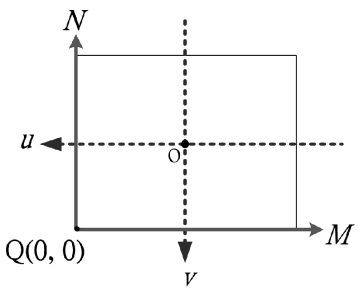

Fig. 3 Relation between M-N image coordinates and u-v image coordinates.

$$\frac{dh_{i12}(v)}{dv} \cong \frac{H_1 \times \lambda}{h} \times \frac{(\tan(\xi) - \tan(\tau)) \times \frac{d(1 + \tan(\xi) \times \tan(\tau))}{dv} - (1 + \tan(\xi) \times \tan(\tau)) \times \frac{d(\tan(\xi) - \tan(\tau))}{dv}}{(\tan(\xi) - \tan(\tau))^2} \tag{15}$$

$$\frac{dh_{i12}(v)}{dv} \cong \frac{H_1 \times \lambda}{h} \times \frac{\left(\tan(\xi) - \frac{v}{\lambda}\right) \times \frac{d\left(1 + \tan(\xi) \times \frac{v}{\lambda}\right)}{dv} - \left(1 + \tan(\xi) \times \frac{v}{\lambda}\right) \times \frac{d\left(\tan(\xi) - \frac{v}{\lambda}\right)}{dv}}{\left(\tan(\xi) - \frac{v}{\lambda}\right)^2} \tag{16}$$

Table 1 Relations between N and Z coordinates.

Parameters		Z-coordinate (Meter)					
		N=0	N=100	N=200	N=300	N=400	N=492
α=0°	λ=8mm	5.715	9.63	30.56	∞	∞	∞
α=0°	λ=16mm	11.43	19.25	61.11	∞	∞	∞
α=2°	λ=8mm	4.91	7.61	16.76	∞	∞	∞
α=2°	λ=16mm	8.71	12.66	23.12	130.82	∞	∞
α=6°	λ=16mm	5.87	7.48	10.26	16.27	38.66	∞
α=8°	λ=16mm	5.03	6.19	8.01	11.29	18.94	49.35

The units of N and Z are the numbers of pixels and meters respectively.

Table 2 Error analysis of range estimation.

Parameters		Error ratio					
		Z=10	Z=20	Z=30	Z=40	Z=50	Z=60
α=0°	λ=8mm	0.36%	0.72%	1.08%	1.44%	1.82%	2.18%
α=0°	λ=16mm	—	0.36%	0.54%	0.72%	0.90%	1.08%
α=2°	λ=8mm	0.36%	0.72%	1.08%	1.44%	1.82%	2.18%
α=2°	λ=16mm	0.18%	0.36%	0.54%	0.72%	0.90%	1.08%

* "—" means beyond the field of view.

7.4(H)×7.4(V) μm, that is $d_x = d_y = 7.4\,\mu$m, the number of pixels is 644×493, and $h = 1.3$ meters. In the analyses, with different camera parameters, Table 1 shows the mapping relation between the N-coordinate and the Z-coordinate based on (26). $N = 0$ is mapped to the smallest Z-coordinate in the field of view. The table shows that the smaller Z-coordinate can be included in the field of view when the focal length is smaller or the tilt angle is larger. When $\alpha = 0^\circ$, the mapping of $N > 246$ is $Z = \infty$. Here ∞ means that the Z-coordinate approaches infinity. Therefore, with a larger α, a smaller Z-coordinate is still in the field of view. The range of the N-coordinate onto which the Z-coordinate is mapped will be relatively larger. For example, the mapping range is $N = [0, 246]$ when $\alpha = 0^\circ$, and $N = [0, 492]$ when $\alpha = 8^\circ$. So a larger α leads to a compact mapping, thus the estimation errors can be accordingly reduced. However, if α is too large, the mapping range of Z shrinks and distant objects are out of the field of view. When $\alpha = 8^\circ$ and $\lambda = 16$ mm, the Z-coordinate will be [5.03, 49.35] meters in the camera's field of view. Hence, it should make the focal length smaller or $\alpha < 8^\circ$, the range of estimation can be larger than 49.35 m.

3.2 Error Estimation

Factors influencing the accuracy of range estimation will be discussed and their impact will be estimated in this section.

3.2.1 Quantization Errors

Image digitization may causes quantization errors, errors in range estimation are particularly caused by spatial quantization, and are within ±1/2 pixels [30], [31]. The results of range estimation are dominated by the projective v-coordinate of P_1. Therefore, the largest quantization error in mapping to the Z-coordinate can be estimated with the condition that the errors of v are within ±1/2 pixels. Based on (26), when $Y = 0$, the range of Z should be between the largest range Z_L and the smallest range Z_S as shown in (27), (28) and e_q the percentage of the largest quantization error is displayed in (29).

Table 2 displays the largest quantization error in the range $Z = [10, 60]$ m with specific α and λ. As can be seen from Table 1, the relation between quantization errors and the N-coordinate can be derived from the relation between Z and N-coordinate. In Table 2, the largest quantization error grows with an increasing Z. The larger the focal length of the camera is, the smaller the quantization errors become. The tilt angle of the camera will not influence the largest quantization error according to the analysis results shown in Table 2.

$$Z_L = h \cdot \tan\left(\left(\frac{\pi}{2} - \alpha\right) - \tan^{-1}\left(\frac{((N_n/2) - N - 0.5) \times d_y}{\lambda}\right)\right) \tag{27}$$

$$Z_S = h \cdot \tan\left(\left(\frac{\pi}{2} - \alpha\right) - \tan^{-1}\left(\frac{((N_n/2) - N + 0.5) \times d_y}{\lambda}\right)\right) \tag{28}$$

$$e_q = \frac{\max(|Z - Z_L|, |Z - Z_S|)}{Z} \tag{29}$$

3.2.2 Influence of Changes in Translation

The analyses of translation can be divided into the directions of X, Y and Z. The origin of the world coordinates is on the ground below the camera, so the Z-coordinate is the range between the preceding vehicle and the camera. Therefore, the subsection will analyze how the changes of X and Y translation influence the range estimation on the Z-coordinate.

X-translation: in (1), the projective position of P_1 onto the v-coordinate determines the Z-coordinate. Figure 2 (b) shows that the changes of X-translation rarely af-

Table 3 Error analysis of range estimation caused by change of tilt angles.

Parameters		Error ratio					
		Z=10	Z=20	Z=30	Z=40	Z=50	Z=60
α=0°	α_1=1°	12.04%	21.25%	28.75%	34.93%	40.17%	44.5%
α=0°	α_1=2°	21.53%	35.10%	44.71%	51.85%	57.36%	61.73%
α=2°	α_1=3°	12.04%	21.25%	28.75%	34.93%	40.17%	44.5%
α=2°	α_1=4°	21.53%	35.10%	44.71%	51.85%	57.36%	61.73%

fect the mapping position of P_1 onto the v-coordinate. So X-translation seldom influences the accuracy of range estimation.

Y-translation: if the ground is flat, the Y-translation of every point on the ground is zero. When the ground is uneven or when the height of the camera is changed because of vibrations, then the initially determined camera height h may be influenced. Let h denote the initially determined height, and h_2 denote the actual height. According to (26), the Z-coordinate mapping result can be obtained by (30). If the original height h is adopted, then the error coming from changes of height will be Z_{dh} in (31) and the error ratio is e_{rh} in (32). Accordingly, errors caused by the Y-translation can be suppressed by increasing the camera height or making the changes of height smaller.

$$Z_{h2} = h_2 \cdot \tan\left(\left(\frac{\pi}{2} - \alpha\right) - \tan^{-1}\left(\frac{((N_n/2) - N) \times d_y}{\lambda}\right)\right) \tag{30}$$

$$Z_{dh} = abs\left((h - h_2) \cdot \tan\left(\left(\frac{\pi}{2} - \alpha\right) - \tan^{-1}\left(\frac{((N_n/2) - N) \times d_y}{\lambda}\right)\right)\right) \tag{31}$$

$$e_{rh} = Z_{dh}/Z_h = (h - h_2)/h \tag{32}$$

3.2.3 Influence of Changes in Camera Tilt Angles

If vibrations cause the tilt angle of the camera to change from α to α_1, the result of mapping is computed by (33). Therefore, if the original α is applied, the error ratio of range estimation caused by changes of tilt angles is $e_{r\alpha}$ in (34).

$$Z_{\alpha 1} = h \cdot \tan\left(\left(\frac{\pi}{2} - \alpha_1\right) - \tan^{-1}\left(\frac{((N_n/2) - N) \times d_y}{\lambda}\right)\right) \tag{33}$$

$$e_{r\alpha} = \frac{|Z_{\alpha 1} - Z|}{Z} \tag{34}$$

To estimate errors caused by tilt angle changes of the camera during the range estimation, let h be 1.3 meters, and focal length λ be 8 mini-meters. The analysis of errors is shown in Table 3. As depicted in Table 3, when both $\alpha = 0^\circ$ and $\alpha = 2^\circ$ have a variation of 1°, the obtained errors are the same. So the initially set tilt angle does not influence the errors of results. However, errors increase when changes of tilt angle grow larger. The error ratio is about 40% at a $Z = 50$ meters at a change of 1° on the tilt angle, revealing that changes of angles significantly affect the results of range estimation. With the same camera parameters but the focal length being changed to 16 mm, the result will remain unchanged, which demonstrates that the focal length is not related to errors arising from changes of tilt angles. This is because when the focal length varies, the estimated range Z and $Z\alpha_1$ will still remain the same, representing that the error ratio will still keep constant.

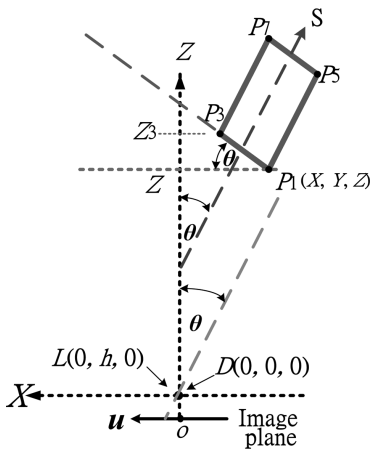

Fig. 4 The relation between the Z-axis and the direction of movement of vehicles, denoted by $\vec{S}$.

Table 4 Variation ratio betweenP_1 and P_3 on the Z-coordinate.

Θ	Z_d (m)	Variation ratio	
		Z=30m	Z=40m
1°	0.024	0.08%	0.006%
5°	0.122	0.41%	0.31%
10°	0.243	0.81%	0.61%

3.2.4 Influence of Changes in Camera Pan Angles

Figure 2 (c) shows the condition that the Z-axis parallels the preceding direction of vehicles, denoted by $\vec{S}$. However, the condition may not be always valid. For example, in Fig. 4, the pan angle between $\vec{S}$ and the Z-axis is θ, the variation between P_1 and P_3 on the Z-coordinate is Z_{dp} as expressed in (35) and the variation ratio is modeled by (36). When the distance between P_1 and P_3 is 1.4 m, the related value of Z_{dp} and the variation ratio are shown in Table 4. In Table 4, the influence turns smaller with a smaller pan angle or a larger range. Even when $\theta = 10^\circ$ and the range is 30 m, the variation ratio is still less than 1%, which shows that pan angles have little influence on the range estimation.

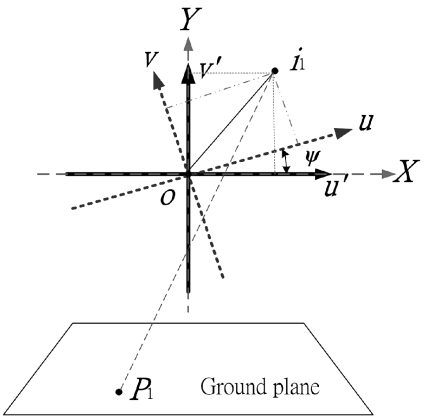

Fig. 5 Relation between the coordinates (u, v) and (u', v').

Table 5 Variations between (u, v) and (u', v').

(u, v)	(u', v')	
	ψ=1°	ψ=2°
(100, 200)	(98.24, 101.73)	(96.45, 103.43)
(200, 200)	(196.48, 203.46)	(192.90, 206.86)

$$Z_{dp} = W_1 \times \cos\theta \tag{35}$$

$$e_{dp} = \frac{Z_{dp}}{Z} \tag{36}$$

3.2.5 Influence of Changes in Camera Swing Angles

The swing angle, i.e. the u-v image plane rotation angle, denotes the angle between the u-axis in the image coordinates and the X-axis in the world coordinates. As shown in Fig. 5, let P_1 project onto i_1 and let i_1 be (u, v) on the u–v plane and (u', v') on the u'–v' plane. (u, v) and (u', v') are the coordinates when $\psi \neq 0$ and $\psi = 0$, respectively. The transformation of the two coordinates can be computed by (37).

$$\begin{bmatrix} u' \\ v' \end{bmatrix} = \begin{bmatrix} \cos\psi & -\sin\psi \\ \sin\psi & \cos\psi \end{bmatrix} \begin{bmatrix} u \\ v \end{bmatrix} \tag{37}$$

If $\psi \neq 0$, from (1), we can obtain the results of range estimation by using (38).

Table 5 shows that the variation between the two coordinates grows with the increasing ψ, u and v. Even if ψ is very small, it still has a great influence when the coordinates are far away from the image center.

$$Z(v) = h{\cdot}\tan\left(\left(\frac{\pi}{2} - \alpha\right) - \tan^{-1}\left(\frac{-\sin\psi \times u + \cos\psi \times v}{\lambda}\right)\right) \tag{38}$$

4. Dynamic Calibration Method

Error estimation shows that the variation of camera swing and tilt angles significantly affects the range estimation results. Therefore, an approach is proposed to reduce estimation errors by automatically calibrating camera angles.

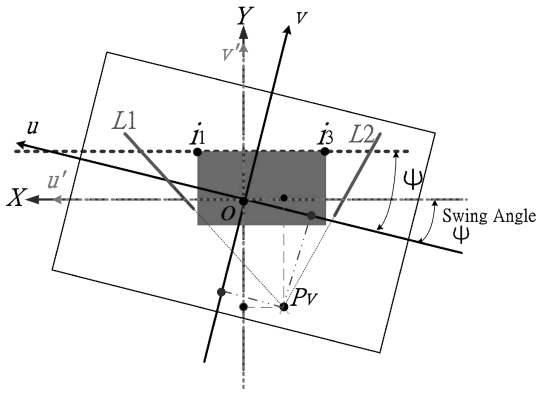

Fig. 6 Projection of a vehicle and lane markings in the image coordinates.

The proposed approach can obtain the swing angle ψ by finding a line that is parallel to the X-axis. In Fig. 4, when the direction of the camera is the same as the moving direction of the preceding vehicle, the camera's pan angle to the vehicle can be reasonably supposed to be zero. Let contact points between the ground and the two rear wheels of the preceding vehicle be P_1 and P_3 as shown in Fig. 2 (a). The world coordinates of the two points have the same Z-coordinate, so $\overline{P_1P_3}$ is parallel to X-axis. In Fig. 6, let P_1 and P_3 respectively project onto i_1 (u, v) and $i_3(u_3, v_3)$. The slope of $\overline{i_1i_3}$ is the same as u'-axis. Then, the angle between $\overline{i_1i_3}$ and *u-axis* is the swing angle ψ. Therefore, ψ can be derived from $i_1(u, v)$ and $i_3(u_3, v_3)$ as computed by (39).

$$\psi = \tan^{-1}\left[(v - v_3)/(u - u_3)\right] \tag{39}$$

The analyses in Table 4 show that when the swing angle $\psi = 0$, even if the camera pan angle $\theta \neq 0$, the Z-coordinates of P_1 and P_3 are still very close and the mapped v-coordinates of the two points are almost the same. So the influence of the pan angle can be neglected and the angle between $\overline{i_1i_3}$ and the *u-axis* can be regarded as the swing angle ψ as shown in Fig. 6.

When the distance between a point on the ground to the camera approaches infinity, its projective point onto the image is named by a vanishing point. When two parallel lines on the ground project to the image coordinates, they tend to converge in a vanishing point. In Fig. 6, let the convergent point of the extended driving markings L_1 and L_2 be $p_v(u_v, v_v)$. Then, p_v is a vanishing point. Suppose that the associated world coordinate of p_v be $P_{vw}(X, 0, Z_v)$ whose range to the camera approaches infinity. Based on (38), we can compute α by (40). Equation (41) is derived according to $Z_v \to \infty$. Equation (42) is formed by substituting (41) into (40). Therefore, we can obtain α by substituting a vanishing point (u_v, v_v) into (42).

$$\alpha = \pi/2 - \tan^{-1}\left[(-\sin\psi \times u_v + \cos\psi \times v_v)/\lambda\right] - \tan^{-1}(Z_v/h) \tag{40}$$

$$\lim_{Z_v \to \infty} \tan^{-1}(Z_v/h) = \pi/2 \tag{41}$$

$$\alpha = -\tan^{-1}\left((-\sin\psi \times u_v + \cos\psi \times v_v)/\lambda\right) \tag{42}$$

5. Application and Experimental Results

The proposed approach can be applied to range and position estimation for vision-based on-road vehicle detection systems.

5.1 Performance Evaluation on Range Estimation

We conduct experiments to compare the differences between the estimated and measured results concerning the range and size of the experimental objects. The height of experimental target is 1 meter; the parameters of the camera, Hitachi KP-F3, were set to be $\alpha = 0°$, $h = 1.3$ m and $\lambda = 10$ mm. An image was taken at every meter at the range of 11–60 meters.

In Fig. 7, the horizontal axis denotes the range between the experimental target and the camera, while the vertical axis represents the contact points between the experimental target and the ground, P_1, which projects onto the N-coordinate. 'Manual' curve shows the result of manual measurement and 'Estimated' is the result of range estimation using (26). The two curves approximately match each other, and these results demonstrate that the proposed range estimation approach yields similar results to those of the actual measurements.

In Fig. 8, the horizontal axis denotes the contact point, P_1, which projects onto the N-coordinate, while the vertical axis indicates the projective height of the experimental target. The figure reveals that the results of manual measurement closely match those of the estimated ones by our proposed method. Figure 9 also reveals that the manually measured results and those estimated by our proposed method are quite close. The experimental target is estimated as 0.98 m by our approach to height estimation, which shows a slight error of 0.02 m when compared with the actual height 1 meter. Those results demonstrate that the proposed approach is efficient in the estimation of vehicle heights and can be used to determine the vehicle sizes.

Figure 9 indicates that the dynamic calibration of angles can improve the accuracy of estimations when the camera angles change. In the experiments, $h = 1.32$ m; $\lambda = 20$ mm; $\alpha = 5°$, $\theta = 0°$; $\psi = 4.8°$. To capture images of a calibrated target, measurements were taken every 5 meters within a distance of 15–50 m. The proposed approach was then applied to estimate the camera's swing angle based on those images. The estimated average of ψ was 4.71°, and the standard deviation was 0.256°. Compared with the setting of $\psi = 4.8°$, the estimation error was about 0.09°. The estimated results and errors of Schoepflin and Dailey's [16] approach in the same case are compared with ours as shown in Table 6, where Schoepflin and Dailey suppose $\psi = 0°$. However, the hypothesis of $\psi = 0°$ differs from the actual situation and thus leads to larger errors in tilt angle estimation. In Fig. 9, curve 'A' shows the difference between manual range measurement and estimated range results using $\alpha = 4.70°$ obtained by Schoepflin and Dailey's approach. The comparison in the 'B' curve uses our approach whose computed $\alpha = 4.93°$. The comparison between curve 'A' and 'B' shows that errors of range estimation are significantly suppressed using our approach.

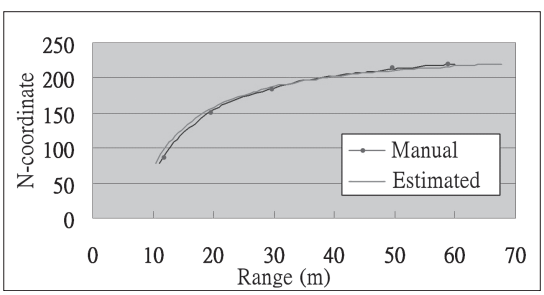

Fig. 7 A comparison between the manual range measurement and the estimated range.

5.2 Simulation Results of Height Estimation

Figure 10 depicts the analytical results of the height estimation. We set the camera height $h = 1.3$ m and the height $\overline{P_1 P_2}$ of the target object to be 1 m; as shown in Fig. 2 (a). Then, as shown in Fig. 10, the horizontal axis represents the projective N-coordinate of P_1 and the vertical axis is the projective height of $\overline{P_1 P_2}$. Lines (A) and (B) show that if $\alpha = 0°$, the changes in focal length seem not to influence the rela-

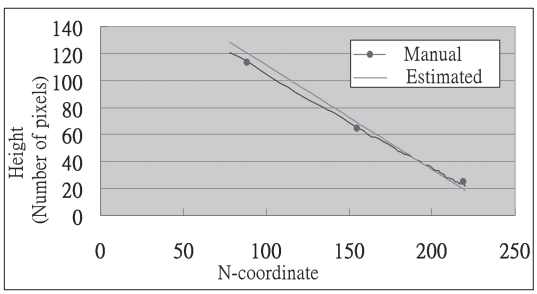

Fig. 8 A comparison between the manual height measurement and the estimated height.

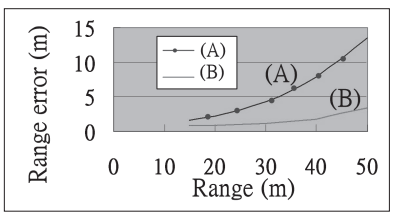

Fig. 9 A comparison of estimation results between Schoepflin's approach and ours.

Table 6 Experimental results of camera angle estimation.

Approach	estimated ψ, error	Estimate α, error
Schoepflin and Dailey [16]	0°, 4.8°	4.70°, 0.30°
Our approach	4.71°, 0.09°	4.93°, 0.07°

tionship between the projective N-coordinate of P_1 and the projective height of $\overline{P_1 P_2}$. Conversely, Lines (C) and (D) display that if $\alpha \neq 0^\circ$, differences in focal length can change their relationship. In Fig. 10, the projective height of $\overline{P_1 P_2}$ varies with the projective position of P_1 in the N-coordinate, and their relationship can be approximated by the linear equation, as in (22). In Fig. 10, the slopes of lines (A) and (B) are the same, -0.769, while in line (C), it is -0.767, and line (D) -0.768. From the proposed approach of fast height estimation in (22), the slope H_1/h, can be estimated to be -0.769, which shows that our fast computation model can provide quite accurate estimation results. The computation using (3) requires 2 tan operations, 2 $\tan^{-1}$ operations, 3 division, 2 multiplications, and 5 deductions, however, our approach needs only 1 multiplication and 1 addition, which obviously promotes executive efficiency.

5.3 Dynamic Calibration of the Swing Angle

The camera mounted on the experimental vehicle is slightly adjusted to an incline of $\psi = 4^\circ$ based on the manual estimation. In the experiments, with the experimental vehicle driving on the road, 500 frames were taken to detect the nearest vehicle in the front driving lane and the contact points between its two rear wheels and the ground. The mean and variance of ψ were estimated to be 3.859° and 0.99°, respectively.

In this study, we analyze errors caused by image digitalization, algorithmic limitations, lens distortion, the vibration of the experimental vehicle, and the uneven surfaces of the roads. The mean and variance obtained by a tracking process with a Kalman filter were 3.861° and 0.58° respectively. In Fig. 11, the curve "Original" is the value of the swing angle derived by the original algorithm without the tracking process. The curve "Kalman" displays the results of utilizing a Kalman filter to improve the robustness of the estimation results. The experiments confirm that the proposed dynamic calibration approach can efficiently and accurately estimate the camera parameters.

5.4 Comparative Performance Evaluation

The proposed approach was compared with the well-known methods shown in Table 7 [15], [17]. Wang and Tsai [15] utilized a hexagon as the calibration target. However, the hexagon is not available under the moving camera, and needs to be pre-determined in the field of view. Conversely, calibration targets applied in other approaches are objects appearing in general traffic scenes, so require no additional effort on manual setting of the calibration target. The camera angle calibration in the range estimation depends only on the tilt α and the swing angle ψ, so only the access to these two angles were compared. Liang et al. [17] assumed that the vanishing point would be in the center of the image, and accordingly estimated an approximate tilt α. Liang et al.'s hypothesis is valid only in the conditions that the location of the camera is in the middle of the driving lane and the lane markings are straight lines. However, even when vehicles are driving on an ideal straight lane, it is still not easy to keep them stably in the center of lanes. Figure 12 (a) and (b) are two cases of comparisons between Liang et al.'s and our approach to estimate the tilt angle. Liang et al. [17] proposed extending the lane markings to search for the vanishing line $V_p(u_v, v_v)$ and estimating α by V_p. In Fig. 12, the convergent point of the u-axis and v-axis is O_i, the center of the image. L_1 and L_2 respectively represent the extensions of the right and left lane markings, and their convergent point is a vanishing point, V_{p1}. Liang et al.'s approach estimated tilt angle by V_{p1}. P_1 and P_3 are the right and left contact points between the preceding vehicle and the ground. The two points are applied to (39) to acquire the swing angle by our methods. The estimated α and estimated errors of camera angles are shown in Table 8, where case 1 and case 2 present

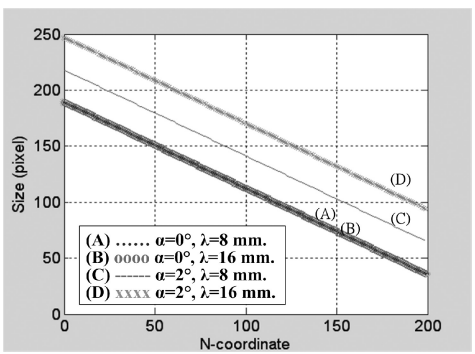

Fig. 10 Estimation of a cuboid's projective height.

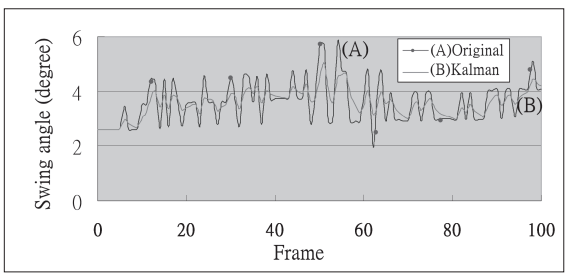

Fig. 11 Dynamic calibration of the swing angle.

Table 7 Comparison of approaches.

Approach	Calibration Target	Calibration angle	Occasion
Wang and Tsai [15]	Hexagon	ψ, α	Fixed camera
Liang *et al.* [17]	Lane marking	Approximation of α	Moving camera
Our approach	Lane marking, Vehicle	ψ, α	Moving camera

Table 8 A comparison in estimation results of camera angle and errors.

Approach	Case 1, ψ=6°; α=3.5°.		Case 2, ψ=0°, α=2.5°	
	α	error	α	error
Liang *et al*. [17]	0.52°	2.98°	2.81°	0.31°
Our approach	3.51°	0.01°	2.29°	0.21°

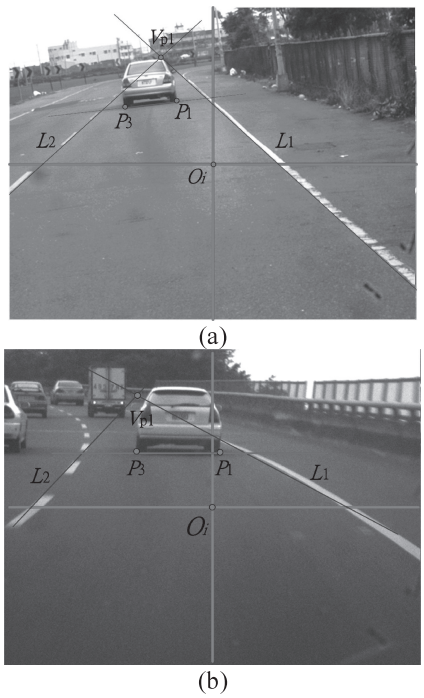

Fig. 12 The swing angle calculated by Liang et al's and our approaches. (a) Straight lane markings. (b) The curve of lane markings.

the situation of Fig. 12 (a) and Fig. 12 (b) respectively. The camera setting in Fig. 12 (a) is $\psi = 6^\circ$ and $\alpha = 3.5^\circ$, and in Fig. 12 (b) is $\psi = 0^\circ$, $\alpha = 2.5^\circ$. As shown in Table 8, the estimated results of tilt angle by Liang et al.'s approach may have larger errors in these cases. That is because the camera is not at the center of the lane, the swing angle is not correctly estimated, and the lane markings are not straight. Comparatively, in our method, the swing angle can be correctly obtained by (39) and then the tilt angle can also be appropriately estimated by (42). Therefore, in these cases, our approach can obtain more accurate results without the limitations due to some pre-determined conditions. Among the three approaches in Table 7, only Liang et al.'s and our approach use calibration targets on the road to achieve dynamic calibration, when the moving camera causes continuously variations of tilt angle α.

6. Conclusions

In this study, we have presented several approaches for the estimation of the range between the preceding vehicle and the camera, range errors, the actual height of vehicles and the projective height of the detected vehicles in various positions. The results of error estimation can be adopted as a reference to determine the preset camera parameters, suppress estimation errors and facilitate rapid and accurate estimation of vehicle sizes.

According to the error analyses, the variations of camera tilt and swing angles lead to significant errors in range estimation results. A dynamic calibration approach has been proposed to effectively reduce errors of range estimation. A Kalman filter is also integrated in order to more stably estimate swing angles so that the estimation results can be sufficiently robust and estimation errors can be further reduced. Experimental results demonstrate that our approaches can provide accurate and robust estimations of range and size of target vehicles. The proposed approaches can serve as reference for designers of vision-based driving assistance systems to improve the efficiency of vehicle detection and range estimation.

Acknowledgments

This research was supported by National Science Council under Grant no. NSC 97-2752-E-009 -012 –PAE and NSC-98-2220-E-468-001.

References

[1] R. Labayrade, J. Douret, J. Laneurit, and R. Chapuis, "A reliable and robust lane detection system based on the parallel use of three algorithms for driving safety assistance," IEICE Trans. Inf. & Syst., vol.E89-D, no.7, pp.2092–2100, July 2006.
[2] H. Sawano and M. Okada, "A road extraction method by an active contour model with inertia and differential features," IEICE Trans. Inf. & Syst., vol.E89-D, no.7, pp.2257–2267, July 2006.
[3] K. Sakurai, S. Kyo, and S. Okazaki, "Overtaking vehicle detection method and its implementation using IMAPCAR highly parallel image processor," IEICE Trans. Inf. & Syst., vol.E91-D, no.7, pp.1899–1905, July 2008.
[4] S.K. Joo, Y. Kim, S.I. Cho, K. Choi, and K. Lee, "Traffic light detection using rotated principal component analysis for video-based car navigation system," IEICE Trans. Inf. & Syst., vol.E91-D, no.12, pp.2884–2887, Dec. 2008.
[5] K. Kanatani, Y. Sugaya, and H. Ackermann, "Uncalibrated factorization using a variable symmetric affine camera," IEICE Trans. Inf. & Syst., vol.E90-D, no.5, pp.851–858, May 2007.
[6] B.F. Wu and C.T. Lin, "Robust image measurement and analysis based on perspective transformation," Proc. IEEE Syst., Man, Cybern. Symp., pp.2390–2395, Oct. 2006.
[7] M. Morimoto and K. Fujii, "A flexible gaze detection method using single PTZ camera," IEICE Trans. Inf. & Syst., vol.E90-D, no.1, pp.199–207, Jan. 2007.
[8] B.F. Wu and C.T. Lin, "Real-time fuzzy vehicle detection based on contour size similarity," Int. J. Fuzzy Systems, vol.7, pp.54–62, June 2005.
[9] H.Y. Lin and J.H. Lin, "A visual positioning system for vehicle or mobile robot navigation," IEICE Trans. Inf. & Syst.,vol.E89-D, no.7, pp.2109–2116, July 2006.

[10] Z. Bian, H. Ishii, H. Shimoda, and M. Izumi, "Real-time tracking error estimation for augmented reality for registration with linecode markers," IEICE Trans. Inf. & Syst., vol.E91-D, no.7, pp.2041–2050, July 2008.
[11] Y. Chen, "Highway overhead structure detection using video image sequences," IEEE Trans. Intell. Trans. Syst., vol.4, no.2, pp.67–77, 2003.
[12] E. Segawa, M. Shiohara, S. Sasaki, N. Hashiguchi, T. Takashima, and M. Tohno, "Preceding vehicle detection using stereo images and non-scanning millimeter-wave radar," IEICE Trans. Inf. & Syst., vol.E89-D, no.7, pp.2101–2108, July 2006.
[13] N. Hautiere, R. Labayrade, and D. Aubert, "Estimation of the visibility distance by stereovision: A generic approach," IEICE Trans. Inf. & Syst., vol.E89-D, no.7, pp.2084–2091, July 2006.
[14] S. Nedevschi, R. Danescu, D. Frentiu, T. Marita, F. Oniga, C. Pocol, R. Schmidt, and T. Graf, "High accuracy stereo vision system for far distance obstacle detection," Proc. IEEE Intelligent Vehicles Symp., pp.292–297, June 2004.
[15] L.L. Wang and W.H. Tsai, "Camera calibration by vanishing lines for 3-D computer vision," IEEE Trans. Pattern Anal. Mach. Intell., vol.13, no.4, pp.370–376, 1991.
[16] T.N. Schoepflin and D.J. Dailey, "Dynamic camera calibration of roadside traffic management cameras for vehicle speed estimation," IEEE Trans. Intell. Trans. Syst., vol.4, no.2, pp.90–98, 2003.
[17] Y.M. Liang, H.R. Tyan, S.L. Chang, H.Y.M. Liao, and S.W. Chen, "Video stabilization for a camcorder mounted on a moving vehicle," IEEE Trans. Veh. Technol., vol.53, no.6, pp.1636–1648, 2004.
[18] Y. Hwang, J. Seo, and H. Hong, "Key-frame selection and an LMedS-based approach to structure and motion recovery," IEICE Trans. Inf. & Syst., vol.E91-D, no.1, pp.114–123, Jan. 2008.
[19] J. Wang, F. Shi, J. Zhang, and Y. Liu, "A new calibration model of camera lens distortion," Pattern Recognit., vol.41, no.2, pp.607–615, Feb. 2008.
[20] B.W. He and Y.F. Li, "Camera calibration from vanishing points in a vision system," Optics & Laser Technology, vol.40, no.3, pp.555–561, April 2008.
[21] K.T. Song and J.C. Tai, "Dynamic calibration of pan–tilt–zoom cameras for traffic monitoring," IEEE Trans. Syst. Man Cybern. B, Cybern., vol.36, no.5, pp.1091–1103, Oct. 2006.
[22] A. Yilmaz, X. Li, and M. Shah, "Contour-based object tracking with occlusion handling in video acquired using mobile cameras," IEEE Trans. Pattern Anal. Mach. Intell., vol.26, no.11, pp.1531–1536, 2004.
[23] S.F. Lin, J.Y. Chen, and H.X. Chao, "Estimation of number of people in crowded scenes using perspective transformation," IEEE Trans. Syst. Man Cybern. A, Syst. Humans, vol.31, no.6, pp.645–654, 2001.
[24] C.C.C. Pang, W.W.L. Lam, and N.H.C. Yung, "A novel method for resolving vehicle occlusion in a monocular traffic-image sequence," IEEE Trans. Intell. Trans. Syst., vol.5, no.3, pp.129–141, 2004.
[25] A. Broggi, M. Bertozzi, L. Guarino, C. Bianco, and A. Piazzi, "Visual perception of obstacle and vehicles for platooning," IEEE Trans. Intell. Trans. Syst., vol.1, no.3, pp.164–176, 2000.
[26] Y.L. Chen, Y.H. Chen, C.J. Chen, and B.F. Wu, "Nighttime vehicle detection for driver assistance and autonomous vehicles," Proc. IAPR International Conference on Pattern Recognition, vol.1, pp.687–690, 2006.
[27] A. Hidaka, K. Nishida, and T. Kurita, "Object tracking by maximizing classification score of detector based on rectangle features," IEICE Trans. Inf. & Syst., vol.E91-D, no.8, pp.2163–2170, Aug. 2008.
[28] B.F. Wu and C.T. Lin, "A fuzzy vehicle detection based on contour size similarity," Proc. IEEE Intelligent Vehicles Symp., pp.495–500, June 2005.
[29] B.-F. Wu and C.-T. Lin, "Robust lane detection and tracking for driving assistance systems," Proc. IEEE Syst., Man, Cybern. Symp., pp.3848–3853, Oct. 2007.
[30] C.C. Yang, M.M. Marefat, and F.W. Ciarallo, "Error analysis and planning accuracy for dimensional measurement in active vision inspection," IEEE Trans. Robot. Autom., vol.14, no.3, pp.476–487, 1998.
[31] B. Kamgar-Parsi and B. Kamgar-Parsi, "Evaluation of quantization error in computer vision," IEEE Trans. Pattern Anal. Mach. Intell., vol.11, no.9, pp.929–939, 1989.

Bing-Fei Wu was born in Taipei, Taiwan in 1959. He received the B.S. and M.S. degrees in control engineering from National Chiao Tung University (NCTU), Hsinchu, Taiwan, in 1981 and 1983, respectively, and the Ph.D. degree in electrical engineering from the University of Southern California, Los Angeles, in 1992. From 1983 to 1984, he was with the Institute of Control Engineering, NCTU as an Assistant Researcher. From 1985 to 1988, he was with the Department of Communication Engineering at the same university as a Lecturer. Since 1992, he has been with the Department of Electrical Engineering and Control Engineering, where he is currently a Professor. As an active industry consultant, he is also involved in the chip design and applications of the flash memory controller and 3C consumer electronics in multimedia. His research interests include chaotic systems, fractal signal analysis, multimedia coding, wavelet analysis and applications.

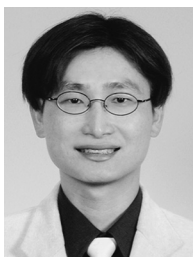

Chuan-Tsai Lin was born in Chunghua, Taiwan, R.O.C., in 1971. He received the B.S. degree in industrial education from the National Chunghua University of Education (NCUE), Chunghua, Taiwan, in 1994, and then received the M.S. degree in electronic engineering from the National Chung Cheng University (NCCU), Chiayi, Taiwan, in 2000. He received the Ph.D. degree in electrical and control engineering from the National Chiao-Tung University, Hsinchu, Taiwan, in 2009. He teaches electronics in Changhua Senior Industrial Vocational High School, NCUE. His research interests include image processing and intelligent transportation system.

Yen-Lin Chen was born in Kaohsiung, Taiwan in 1978. He received the B.S. and Ph.D. degrees in electrical and control engineering from National Chiao Tung University, Hsinchu, Taiwan, in 2000 and 2006, respectively. From Feb. 2007 to Jul. 2009, he was an Assistant Professor at the Dept. of Computer Science and Information Engineering, Asia University, Taichung, Taiwan. Since Aug. 2009, he is now an Assistant Professor at the Dept. of Computer Science and Information Engineering, National Taipei University of Technology, Taipei, Taiwan. He is a member of the IEEE and IAPR. In 2003, he received Dragon Golden Paper Award sponsored by the Acer Foundation and the Silver Award of Technology Innovation Competition sponsored by the AdvanTech. His research interests include image and video processing, pattern recognition, document image analysis, and intelligent transportation system.